Standard Model Higgs Boson with the L3 Experiment at LEP

P. Achard, O. Adriani, M. Aguilar-Benitez, J. Alcaraz, G. Alemanni, J. Allaby, A. Aloisio, M.G. Alviggi, H. Anderhub, V.P. Andreev, et al.

EUROPEAN ORGANIZATION FOR NUCLEAR RESEARCH

CERN-EP/2001-049
July 10, 2001

Standard Model Higgs Boson with the L3 Experiment at LEP

L3 Collaboration

Abstract

Final results of the search for the Standard Model Higgs boson are presented for the data collected by the L3 detector at LEP at centre-of-mass energies up to about 209 GeV. These data are compared with the expectations of Standard Model processes for Higgs boson masses up to 120 GeV. A lower limit on the mass of the Standard Model Higgs boson of 112.0 GeV is set at the 95% confidence level. The most significant high mass candidate is a H$\nu\bar{\nu}$ event. It has a reconstructed Higgs mass of 115 GeV and it was recorded at $\sqrt{s} = 206.4$ GeV.

To be submitted to *Phys. Lett. B*

1 Introduction

One of the most important goals of the L3 experiment at the LEP e^+e^- collider was to find the Higgs boson. In the Standard Model this particle is associated to the Higgs field [1], expected to provide mass to all the observed elementary particles. The mass of the Higgs boson, m_H, is not predicted by the theory. Before the advent of LEP, there was no solid experimental information about the Higgs mass. The L3 experiment has carried out the search for the Higgs boson at LEP in very large data samples collected at the Z resonance [2] and at ever increasing centre-of-mass energies and luminosities [3–7] greatly extending the Higgs mass range investigated.

A fit that includes L3 electroweak precision measurements results in an upper limit on m_H of 133 GeV [8] at the 95% confidence level. Previous L3 direct searches for the Standard Model Higgs boson excluded the mass range up to 107 GeV [6]. Similar results were also reported by other LEP experiments [9]. Results of the Standard Model Higgs search obtained shortly after the end of the LEP data taking in the year 2000 were also published by L3 [7] and by the other LEP experiments [10].

The Standard Model Higgs boson is produced at LEP mainly via the Higgs-strahlung process $e^+e^- \to Z^* \to HZ$. The processes of W^+W^- and ZZ fusion contribute, with smaller rate, to the Higgs production in the $H\nu\bar{\nu}$ and He^+e^- channels, respectively. The largest sources of background are four-fermion final states from W and Z pair production, as well as quark pair production $e^+e^- \to q\bar{q}(\gamma)$.

In this letter, the final results of the Standard Model Higgs search performed on the data collected by L3 at LEP at a centre-of-mass energy, $\sqrt{s}$, up to about 209 GeV are reported. These results include the full luminosity collected in the year 2000 and the corrected LEP beam energies. In the year 2000 LEP was run at several values of $\sqrt{s}$. The slight beam energy adjustments significantly affect the signal expectation at the highest Higgs masses, close to the kinematic limit for HZ production, $m_H = \sqrt{s} - m_Z$, where m_Z is the Z boson mass. The effect of the Z width in the Higgs mass reconstruction close to the HZ kinematic limit is also taken into account. Final calibrations of all subdetectors are applied. The signal and background expectations are evaluated on a finer grid of $\sqrt{s}$ values, with larger samples of simulated events, thus reducing statistical and systematic uncertainties. Therefore, the results reported in this letter are affected by total uncertainties smaller than in Reference 7.

2 Data and Monte Carlo samples

The data were collected by the L3 detector [11] at LEP during the year 2000 at several centre-of-mass energies. The total collected luminosity amounts to 217.3 pb^{-1}. The data are grouped into seven samples corresponding to average centre-of-mass energies between 202.8 GeV and 208.6 GeV. The integrated luminosities corresponding to these samples are given in Table 1.

The Higgs production cross sections and branching ratios are calculated using the HZHA generator [12]. Efficiencies are determined using Monte Carlo samples of Higgs events, generated with PYTHIA [13]. Since the Higgs production cross sections and efficiencies depend strongly on $\sqrt{s}$, in particular for m_H close to the HZ kinematic limit, samples of Higgs events are simulated at each centre-of-mass energy shown in Table 1. Higgs events are generated with m_H between 105 and 120 GeV, in steps of 1 GeV. For each mass and each search channel, between 2000 and 10000 events are generated.

The Standard Model background estimates rely on the following Monte Carlo programs: KK2f [14] for $e^+e^- \to q\bar{q}(\gamma)$, KORALW [15] for $e^+e^- \to W^+W^-$, PHOJET [16] for two-photon

processes ($e^+e^- \to e^+e^-q\bar{q}$) and EXCALIBUR [17] for other four-fermion final states. The number of simulated events for the dominant backgrounds is at least 100 times the number of events expected for such processes.

The response of the L3 detector is simulated using the GEANT program [18], taking into account the effects of multiple scattering, energy loss and showering in the detector. Hadronic interactions in the detector are modelled using the GHEISHA program [19]. Time dependent detector inefficiencies, as monitored during the data taking period, are also simulated.

3 Analysis procedures

The search for the Standard Model Higgs boson is based on the study of four distinct event topologies: $HZ \to q\bar{q}q\bar{q}$, $HZ \to q\bar{q}\nu\bar{\nu}$, $HZ \to q\bar{q}\ell^+\ell^-$ ($\ell = e, \mu, \tau$) and $HZ \to \tau^+\tau^-q\bar{q}$.
In the following they are denoted as $Hq\bar{q}$, $H\nu\bar{\nu}$, $H\ell^+\ell^-$ and $\tau^+\tau^-q\bar{q}$, respectively. With the exception of the $HZ \to \tau^+\tau^-q\bar{q}$ decay mode, all the analyses are optimised for the $H \to b\bar{b}$ decay. This mode represents about 80% of the Higgs branching fraction in the mass range of interest.

All the search channels are analysed in three stages. First, a high multiplicity hadronic event selection is applied to reduce the large background from two-photon processes, while preserving most of the Higgs signal. In a second stage, topological and kinematical variables together with b-tag variables are either used to construct an event likelihood or fed into a neural network, to further discriminate between signal and background events. A b-tag variable is calculated for each hadronic jet using a neural network [3] which exploits three-dimensional decay lengths, properties of semileptonic b decays and jet-shape variables. The event b-tag variable is then obtained as a combination of the b-tag variable for each hadronic jet. The tracking and b-tagging performance in the Monte Carlo simulation are tuned using 4 pb^{-1} of calibration data collected at $\sqrt{s} \sim m_Z$ in the year 2000. The b-tagging performance for the high-energy data is verified with samples of $e^+e^- \to q\bar{q}(\gamma)$ events. The efficiency for tagging light flavoured hadrons is verified with $W^+W^- \to q\bar{q}\ell\bar{\nu}$ events. The agreement of data with the simulation of Standard Model processes in the event b-tag variable is shown in Figure 1 for the $e^+e^- \to q\bar{q}(\gamma)$ and the $W^+W^- \to q\bar{q}\ell\bar{\nu}$ events. The expectation from the Standard Model Monte Carlo describes the data within the statistical uncertainty.

The last part of the analysis is the construction of a final discriminant for each topology. It is built from a combination of the event likelihood, or the neural network output, with the reconstructed Higgs mass. For each Higgs mass hypothesis, the final discriminants are computed for the data and for the expected background and signal. The distributions of the final discriminants are then used to calculate the likelihood ratio, Q, as a function of m_H. This is the ratio of the probability of observing the data in the presence of both the signal and the background, "signal+background" hypothesis, to the probability of observing the data in the presence of only the background, "background-only" hypothesis. The quantity used to evaluate the compatibility of the data with the signal is the log-likelihood ratio defined by [20]:

$$-2\ln Q \equiv 2\sum_i [s_i - n_i \ln(1 + s_i/b_i)] \ .$$

In this expression, i indicates the i-th bin of the final discriminant of each channel and at each $\sqrt{s}$; n_i, s_i and b_i indicate respectively the number of observed events, the expected Higgs signal and the Standard Model background, in the i-th bin. Each event in the sum has a weight $\ln(1 + s/b)$ which depends on the signal-to-background ratio, s/b, in the bin where it is found. This weight depends on the Higgs mass hypothesis. For each given m_H, the value of the

log-likelihood ratio in the data is compared to the expected distributions of $-2\ln Q$ in a large number of simulated experiments under the "background-only" and the "signal+background" hypotheses. The results for each search channel are then presented in terms of $-2\ln Q$ for the data compared to the expected median values for the two hypotheses, as a function of m_{H}.

3.1 The Hq$\bar{\mathrm{q}}$ analysis

The Hq$\bar{\mathrm{q}}$ analysis aims to select and study events with four jets, two of which contain b hadrons, while the other two must be consistent with the decay of a Z boson. Background from Standard Model processes comes mainly from q$\bar{\mathrm{q}}$ final states with hard gluon radiation, $\mathrm{W^+W^-}$ and ZZ events, especially those where one of the Z bosons decays into b quarks.

After a high multiplicity hadronic preselection, the events are forced into four jets with the DURHAM algorithm [21] and a kinematic fit requiring four-momentum conservation is performed. Several discriminating variables, x_i, are combined into a single likelihood which is then used to select the final sample. In this combination, each final state is considered as an event class j (j=HZ, ZZ, WW, q$\bar{\mathrm{q}}$). For each class, probability density functions $f^j(x_i)$ are derived from Monte Carlo. The probability for an event to belong to the event class j, based on the value of the variable x_i, is defined as $p^j(x_i) = f^j(x_i)/\sum_k f^k(x_i)$, where k runs over all classes.

The individual probabilities are combined into a likelihood: $L_{\mathrm{HZ}} = \prod_i p^{\mathrm{HZ}}(x_i)/\sum_k \prod_i p^k(x_i)$, where i runs over all variables considered and k over all event classes. Ten variables are used to calculate the likelihood. They are:

- the number of tracks,
- the event b-tag,
- the maximum energy difference between any two jets,
- the minimum jet energy,
- the parameter of the DURHAM algorithm for which the event is resolved from three jets into four jets,
- the maximal triple-jet boost, defined as the maximum three-jet boost obtained from the four possibilities to construct a one-jet against three-jet configuration in a four-jet event,
- the minimum opening angle between any two jets,
- the event sphericity,
- the mass from a 5C kinematic fit imposing energy and momentum conservation and equal dijet masses, M_{eq}^{5C},
- the absolute value of the cosine of the production polar angle, $|\cos\Theta|$, assuming the production of a pair of bosons.

The distributions of the event b-tag, M_{eq}^{5C}, $|\cos\Theta|$ and L_{HZ} for the events selected in the Hq$\bar{\mathrm{q}}$ search channel with $\sqrt{s} > 206$ GeV, compared to the expectation for Standard Model processes, are shown in Figure 2.

Events are selected into the final sample if the value of L_{HZ} exceeds a threshold optimised for each centre-of-mass energy and each Higgs mass hypothesis. In addition, the compatibility of each event with a Higgs mass hypothesis m_{H} is tested by the variable $\chi^2_{\mathrm{HZ}} = \big(\Sigma_i - (m_{\mathrm{H}} + m_{\mathrm{Z}})\big)^2/\sigma^2_{\Sigma_{\mathrm{HZ}}} + \big(\Delta_i - |m_{\mathrm{H}} - m_{\mathrm{Z}}|\big)^2/\sigma^2_{\Delta_{\mathrm{HZ}}}$. In this expression, Σ_i and Δ_i are the dijet mass sum and dijet mass difference, respectively, for the i-th of the three possible jet pairing combinations, while $\sigma_{\Sigma_{\mathrm{HZ}}}$ and $\sigma_{\Delta_{\mathrm{HZ}}}$ are the corresponding resolutions for Higgs events. The jet pairing with the best χ^2 is chosen. Finally, only events with the χ^2 probability above 0.01 are selected. As an example, for $m_{\mathrm{H}} = 110$ GeV, 179 events are selected in the data with 172 expected from background processes and 12.8 events expected from the Higgs signal; for $m_{\mathrm{H}} = 115$ GeV, 149 events are observed with 142 from background and 3.2 from the Higgs signal.

For these events a final discriminant is constructed. At first, the events are classified into three categories depending on the values of the b-tag of the two jets assigned to the Higgs boson. The first category contains events where none of these jets has the highest value of the b-tag among the four jets of the event. The second category is composed of events where one of these jets has the highest b-tag value. The third category contains events where the two jets assigned to the Higgs boson have the highest b-tag values. The χ^2_{HZ} probability, the b-tag values of the individual jets and the event category are then combined into the final discriminant.

3.2 The H$\nu\bar{\nu}$ analysis

The H$\nu\bar{\nu}$ search is based on the selection of events with two jets containing b hadrons, with large missing energy and missing mass consistent with m_{Z}. A neural network is used for the H$\nu\bar{\nu}$ analysis, very similar to the one previously reported [6, 7]. However, tighter cuts on radiative photons and on the jet polar angle are applied to reduce the $\mathrm{e^+e^-} \to \mathrm{q\bar{q}}(\gamma)$ background and ensure the best jet energy and b-tag measurements. The signal efficiency is slightly reduced by a few percent relative but the search performance is not significantly modified. In addition, the neural network is trained with the final, high statistics, signal and background Monte Carlo samples, at each $\sqrt{s}$ value, to maximise the sensitivity of the analysis.

In the first step of the analysis, high multiplicity hadronic events are selected and forced into two jets using the DURHAM algorithm. The dijet invariant mass must exceed 40 GeV. These requirements reduce contributions from two-photon interactions, while retaining a significant fraction of hadronic events from $\mathrm{e^+e^-} \to \mathrm{q\bar{q}}(\gamma)$ and W-pair production. These backgrounds are then reduced by requiring the visible mass to be less than 140 GeV and the mass recoiling against the hadronic system to lie between 50 GeV and 130 GeV.

Events from $\mathrm{e^+e^-} \to \mathrm{q\bar{q}}(\gamma)$ are further suppressed by requiring the longitudinal missing energy to be less than $0.6\sqrt{s}$ and the missing momentum vector to be at least 16° away from the beam axis. The energy in the forward luminosity calorimeter is required to be below 20 GeV. The acollinearity is required to be smaller than 65°. The distribution of the event b-tag after the above cuts is shown in Figure 3 a. A loose cut requiring the event b-tag to be larger than 0.5 is then applied, without further loss of signal efficiency. After this set of cuts, there are 123 events in the data, while 130 are expected from background processes with 4.3 and 1.3 events expected for $m_{\mathrm{H}} = 110$ GeV and 115 GeV, respectively.

A kinematic fit imposing four-momentum conservation and requiring the missing mass to be consistent with m_{Z} is performed to compute the reconstructed Higgs mass from the two jets. The output of a mass independent neural network [4] is then combined with the reconstructed Higgs mass to build the final discriminant. The distributions of the reconstructed Higgs mass, the missing mass and the neural network output for the events selected in the H$\nu\bar{\nu}$ search

channel with $\sqrt{s} > 206$ GeV, compared to the expectation for Standard Model processes, are shown in Figure 3. General agreement between the data and the expected contributions from Standard Model processes is observed in all the distributions.

3.3 The $H\ell^+\ell^-$ and $\tau^+\tau^-q\bar{q}$ analyses

The signatures for the He^+e^- and $H\mu^+\mu^-$ processes are a pair of high energy electrons or muons with an invariant mass compatible with m_Z and two hadronic jets with b quark content. In $H\tau^+\tau^-$ events the tau pair invariant mass must also be compatible with m_Z. For these events, the mass resolution is worse than in the other $H\ell^+\ell^-$ channels due to the missing neutrinos from the tau decays. Events with Higgs decaying into tau leptons, $\tau^+\tau^-q\bar{q}$, have similar signature to the $H\tau^+\tau^-$ events, with the difference that the hadronic jet mass must be compatible with m_Z and that the b-tag content of the event is reduced.

The analyses are very similar to those described in Reference 6. The selections require high multiplicity events. In the He^+e^- and $H\mu^+\mu^-$ analyses two well identified electrons or muons are also required. In the tau analyses, tau leptons are identified either by their decay into electrons or muons, or as an isolated low-multiplicity jet with one or three tracks and unit charge. The identified leptons must have a large opening angle and must be well isolated from the hadronic jets. For all $H\ell^+\ell^-$ selections, the invariant mass of the leptons after a kinematic fit imposing four-momentum conservation must be consistent with m_Z within a mass range depending on the dilepton mass resolution. In the $\tau^+\tau^-q\bar{q}$ selection the mass of the two hadronic jets after kinematic fit must be consistent with m_Z.

After the $H\ell^+\ell^-$ selection, 18 events are observed with 16.7 expected from background processes and 1.7 or 0.32 signal events expected for m_H =110 GeV or 115 GeV, respectively. After the $\tau^+\tau^-q\bar{q}$ selection, 8 events are observed with 7.8 expected from background and 0.66 or 0.15 signal events expected for m_H =110 GeV or 115 GeV, respectively.

The distributions of the dilepton mass and the reconstructed Higgs mass in the He^+e^- and $H\mu^+\mu^-$ channels are shown in Figure 4a and 4b. The distributions of the reconstructed Higgs mass in the $H\tau^+\tau^-$ and $\tau^+\tau^-q\bar{q}$ channels are shown in Figure 4c and 4d, respectively.

In the $H\ell^+\ell^-$ selections, the dijet mass after the fit is combined with the b-tag values of the two jets, to form the final discriminant. For the $\tau^+\tau^-q\bar{q}$ selection, the mass of the tau pair, calculated by constraining the invariant mass of the two other jets to m_Z, is used as the final discriminant.

4 Results

Figure 5 shows the observed $-2\ln Q$ compared to the expectation for the "background-only" and the "signal+background" hypotheses, as a function of m_H, for each of the search channels. An observed value of $-2\ln Q$ larger than the median expected value for the background indicates a deficit of events with respect to the expected background while an observed $-2\ln Q$ value below the median expected background value indicates an excess. Good agreement between the observation and the expected background is observed in all channels within one standard deviation from the background expectation. A slight excess of events above one standard deviation from the background is observed in the $H\nu\bar{\nu}$ channel for m_H above 100 GeV. The observed and expected log-likelihood ratio $-2\ln Q$ for all channels combined as a function of m_H is shown in Figure 6.

These results are used to evaluate confidence levels for the "background-only" and the "signal+background" hypotheses. The confidence level for the "background-only" hypothesis, $1 - \mathrm{CL}_b$ [20], is the probability of observing in a large sample of simulated "background-only" experiments a more signal-like value of the log-likelihood ratio than is actually observed. The distribution of $1 - \mathrm{CL}_b$ in a large sample of "background-only" experiments is uniform between 0 and 1, thus its median expected value is 0.5. An observed value of $1 - \mathrm{CL}_b$ lower than 0.5 indicates an excess of events in data compared to the expected background. Similarly, the "signal+background" confidence level CL_{s+b} is defined as the probability in a sample of "signal+background" experiments of observing a less signal-like value of the log-likelihood ratio than is actually observed. To exclude a signal, an additional quantity is defined, $\mathrm{CL}_s = \mathrm{CL}_{s+b}/\mathrm{CL}_b$ [20]. The signal hypothesis is excluded at 95% confidence level when CL_s has a value smaller or equal to 5%.

The statistical and systematic uncertainties on the signal and background expectations are included in the calculations of the combined confidence levels. Statistical uncertainties on the background and signal predictions, arising from the finite number of generated Monte Carlo events, are evaluated to be up to 8% for the background and 4% for the signal. The systematic uncertainties are derived using a similar procedure to the one adopted in previous Standard Model Higgs searches [6]. In addition, a systematic uncertainty on the $\mathrm{q\bar{q}}$ background, which affects mostly the search region close to the HZ kinematic limit in the $\mathrm{H}\nu\bar{\nu}$ and $\mathrm{Hq\bar{q}}$ channels, is included depending on m_{H}. Thus the systematic uncertainty on the number of background events is estimated to be from 6% up to 15% for m_{H} close and beyond the HZ kinematic limit. The systematic uncertainty on the number of signal events is estimated to be between 3% and 6%, for m_{H} close to and beyond the HZ kinematic limit, to take into account the spread of $\sqrt{s}$ values in the different data samples.

The statistical uncertainty is uncorrelated from bin to bin in the final discriminant distributions and has little effect on the confidence level. Bins of the final discriminant distributions with a s/b ratio below 0.05 are not considered in the calculation of the confidence levels, as they degrade the search sensitivity once systematic uncertainties are included in the calculation. The number of selected and expected events for all the analyses after such a s/b cut are summarised in Table 2 for the data, the background and the Higgs signals for $m_{\mathrm{H}} = 110$ GeV and 115 GeV. The number of signal events includes cross-efficiencies from other channels, fusion processes and charm and gluonic Higgs decays.

The confidence level for the "background-only" hypothesis 1-CL_b and the confidence level for the signal hypothesis CL_s as a function of m_{H} are shown in Figure 7. They are computed following the procedure of Reference 20. The results of the L3 Standard Model Higgs searches at lower centre-of-mass energies [5,6] are included in the calculation of these confidence levels. Values of m_{H} below 107 GeV are excluded in the Standard Model with a confidence level greater than 99.5%.

The observed lower limit on m_{H} is 112.0 GeV at the 95% confidence level, for an expected lower limit of 112.4 GeV. This new value improves upon and supersedes our previously published limit. For $m_{\mathrm{H}} = 112.0$ GeV, where CL_s is 5%, the background probability 1-CL_b is 40%. For $m_{\mathrm{H}} = 115$ GeV, the background probability is 32%. The previously published background probability estimates [7] are consistent with the final results presented here, given the size of the uncertainties affecting the signal and background estimate in the vicinity of the kinematic limit.

The most significant candidate for $m_{\mathrm{H}} = 115$ GeV is a $\mathrm{H}\nu\bar{\nu}$ event. It has a reconstructed Higgs mass of 115 GeV and it was recorded at $\sqrt{s} = 206.4$ GeV. The kinematic properties of

this event were described in detail in Reference 7.

Acknowledgements

We acknowledge the efforts of the engineers and technicians who have participated in the construction and maintenance of L3 and express our gratitude to the CERN accelerator divisions for the superb performance of LEP.

References

[1] P. W. Higgs, Phys. Lett. **12** (1964) 132; F. Englert and R. Brout, Phys. Rev. Lett. **13** (1964) 321; G. S. Guralnik *et al.*, Phys. Rev. Lett. **13** (1964) 585.

[2] L3 Collaboration, B. Adeva *et al.*, Phys. Lett. **B 248** (1990) 203; L3 Collaboration, B. Adeva *et al.*, Phys. Lett. **B 252** (1990) 518; L3 Collaboration, B. Adeva *et al.*, Phys. Lett. **B 257** (1991) 450; L3 Collaboration, B. Adeva *et al.*, Phys. Lett. **B 283** (1992) 454; L3 Collaboration, B. Adeva *et al.*, Phys. Lett. **B 303** (1993) 391; L3 Collaboration, M. Acciarri *et al.*, Phys. Lett. **B 383** (1996) 487.

[3] L3 Collaboration, M. Acciarri *et al.*, Phys. Lett. **B 411** (1997) 373.

[4] L3 Collaboration, M. Acciarri *et al.*, Phys. Lett. **B 431** (1998) 437.

[5] L3 Collaboration, M. Acciarri *et al.*, Phys. Lett. **B 461** (1999) 376.

[6] L3 Collaboration, M. Acciarri *et al.*, Phys. Lett. **B 508** (2001) 225.

[7] L3 Collaboration, M. Acciarri *et al.*, Phys. Lett. **B 495** (2000) 18.

[8] L3 Collaboration, M. Acciarri *et al.*, Eur. Phys. J. **C16** (2000) 1.

[9] ALEPH Collaboration, R. Barate *et al.*, Phys. Lett. **B 499** (2001) 53.

[10] ALEPH Collaboration, R. Barate *et al.*, Phys. Lett. **B 495** (2000) 1; DELPHI Collaboration, P. Abreu *et al.*, Phys. Lett. **B 499** (2001) 23; OPAL Collaboration, G. Abbiendi *et al.*, Phys. Lett. **B 499** (2001) 38.

[11] L3 Collaboration, B. Adeva *et al.*, Nucl. Inst. Meth. **A 289** (1990) 35; J. A. Bakken *et al.*, Nucl. Inst. Meth. **A 275** (1989) 81; O. Adriani *et al.*, Nucl. Inst. Meth. **A 302** (1991) 53; B. Adeva *et al.*, Nucl. Inst. Meth. **A 323** (1992) 109; K. Deiters *et al.*, Nucl. Inst. Meth. **A 323** (1992) 162; M. Chemarin *et al.*, Nucl. Inst. Meth. **A 349** (1994) 345; M. Acciarri *et al.*, Nucl. Inst. Meth. **A 351** (1994) 300; G. Basti *et al.*, Nucl. Inst. Meth. **A 374** (1996) 293; A. Adam *et al.*, Nucl. Inst. Meth. **A 383** (1996) 342; L3 Collaboration, O. Adriani *et al.*, Phys. Rep. **236** (1993) 1.

[12] P. Janot, "The HZHA generator", in "Physics at LEP2", CERN Report 96-01 (1996).

[13] PYTHIA versions 5.722 and 6.1 are used.
T. Sjöstrand, Preprint CERN-TH/7112/93 (1993), revised August 1995; Comp. Phys. Comm. **82** (1994) 74; Preprint hep-ph/0001032 (2000)..

[14] KK2f version 4.13 is used;
S. Jadach, B.F.L. Ward and Z. Wąs, Comp. Phys. Comm. **130** (2000) 260.

[15] KORALW version 1.33 is used.
S. Jadach *et al.*, Comp. Phys. Comm. **94** (1996) 216;
S. Jadach *et al.*, Phys. Lett. **B 372** (1996) 289.

[16] PHOJET version 1.05 is used.
R. Engel, Z. Phys. **C 66** (1995) 203;
R. Engel and J. Ranft, Phys. Rev. **D 54** (1996) 4244.

[17] F.A. Berends, R. Kleiss and R. Pittau, Comp. Phys. Comm. **85** (1995) 437.

[18] GEANT Version 3.15 is used,
R. Brun *et al.*, Preprint CERN-DD/EE/84-1 (1984), revised 1985.

[19] H. Fesefeldt, Preprint PITHA 85/02, RWTH Aachen (1985)..

[20] LEP Working Group for Higgs Boson Searches and ALEPH, DELPHI, L3, OPAL Collaborations, "Searches for Higgs bosons: preliminary combined results using LEP data collected at energies up to 202 GeV", Preprint CERN-EP/2000-55 (2000).

[21] S. Catani *et al.*, Phys. Lett. **B 269** (1991) 432; S. Bethke *et al.*, Nucl. Phys. **B 370** (1992) 310.

The L3 Collaboration:

P.Achard,[20] O.Adriani,[17] M.Aguilar-Benitez,[24] J.Alcaraz,[24,18] G.Alemanni,[22] J.Allaby,[18] A.Aloisio,[28] M.G.Alviggi,[28] H.Anderhub,[47] V.P.Andreev,[6,33] F.Anselmo,[9] A.Arefiev,[27] T.Azemoon,[3] T.Aziz,[10,18] M.Baarmand,[25] P.Bagnaia,[38] A.Bajo,[24] G.Baksay,[16] L.Baksay,[25] S.V.Baldew,[2] S.Banerjee,[10] Sw.Banerjee,[4] A.Barczyk,[47,45] R.Barillère,[18] P.Bartalini,[22] M.Basile,[9] N.Batalova,[44] R.Battiston,[32] A.Bay,[22] F.Becattini,[17] U.Becker,[14] F.Behner,[47] L.Bellucci,[17] R.Berbeco,[3] J.Berdugo,[24] P.Berges,[14] B.Bertucci,[32] B.L.Betev,[47] M.Biasini,[32] M.Biglietti,[28] A.Biland,[47] J.J.Blaising,[4] S.C.Blyth,[34] G.J.Bobbink,[2] A.Böhm,[1] L.Boldizsar,[13] B.Borgia,[38] D.Bourilkov,[47] M.Bourquin,[20] S.Braccini,[20] J.G.Branson,[40] F.Brochu,[4] A.Buijs,[43] J.D.Burger,[14] W.J.Burger,[32] X.D.Cai,[14] M.Capell,[14] G.Cara Romeo,[9] G.Carlino,[28] A.Cartacci,[17] J.Casaus,[24] F.Cavallari,[38] N.Cavallo,[35] C.Cecchi,[32] M.Cerrada,[24] M.Chamizo,[20] Y.H.Chang,[49] M.Chemarin,[23] A.Chen,[49] G.Chen,[7] G.M.Chen,[7] H.F.Chen,[21] H.S.Chen,[7] G.Chiefari,[28] L.Cifarelli,[39] F.Cindolo,[9] I.Clare,[14] R.Clare,[37] G.Coignet,[4] N.Colino,[24] S.Costantini,[38] B.de la Cruz,[24] S.Cucciarelli,[32] T.S.Dai,[14] J.A.van Dalen,[30] R.de Asmundis,[28] P.Déglon,[20] J.Debreczeni,[13] A.Degré,[4] K.Deiters,[45] D.della Volpe,[28] E.Delmeire,[20] P.Denes,[36] F.DeNotaristefani,[38] A.De Salvo,[47] M.Diemoz,[38] M.Dierckxsens,[2] D.van Dierendonck,[2] C.Dionisi,[38] M.Dittmar,[47,18] A.Doria,[28] M.T.Dova,[11,♯] D.Duchesneau,[4] P.Duinker,[2] B.Echenard,[20] A.Eline,[18] H.El Mamouni,[23] A.Engler,[34] F.J.Eppling,[14] A.Ewers,[1] P.Extermann,[20] M.A.Falagan,[24] S.Falciano,[38] A.Favara,[31] J.Fay,[23] O.Fedin,[33] M.Felcini,[47] T.Ferguson,[34] H.Fesefeldt,[1] E.Fiandrini,[32] J.H.Field,[20] F.Filthaut,[30] P.H.Fisher,[14] W.Fisher,[36] I.Fisk,[40] G.Forconi,[14] K.Freudenreich,[47] C.Furetta,[26] Yu.Galaktionov,[27,14] S.N.Ganguli,[10] P.Garcia-Abia,[5,18] M.Gataullin,[31] S.Gentile,[38] S.Giagu,[38] Z.F.Gong,[21] G.Grenier,[23] O.Grimm,[47] M.W.Gruenewald,[8,1] M.Guida,[39] R.van Gulik,[2] V.K.Gupta,[36] A.Gurtu,[10] L.J.Gutay,[44] D.Haas,[5] D.Hatzifotiadou,[9] T.Hebbeker,[8,1] A.Hervé,[18] J.Hirschfelder,[34] H.Hofer,[47] G. Holzner,[47] S.R.Hou,[49] Y.Hu,[30] B.N.Jin,[7] L.W.Jones,[3] P.de Jong,[2] I.Josa-Mutuberría,[24] D.Käfer,[1] M.Kaur,[15] M.N.Kienzle-Focacci,[20] J.K.Kim,[42] J.Kirkby,[18] W.Kittel,[30] A.Klimentov,[14,27] A.C.König,[30] M.Kopal,[44] V.Koutsenko,[14,27] M.Kräber,[47] R.W.Kraemer,[34] W.Krenz,[1] A.Krüger,[46] A.Kunin,[14,27] P.Ladron de Guevara,[24] I.Laktineh,[23] G.Landi,[17] M.Lebeau,[18] A.Lebedev,[14] P.Lebrun,[23] P.Lecomte,[47] P.Lecoq,[18] P.Le Coultre,[47] H.J.Lee,[8] J.M.Le Goff,[18] R.Leiste,[46] P.Levtchenko,[33] C.Li,[21] S.Likhoded,[46] C.H.Lin,[49] W.T.Lin,[49] F.L.Linde,[2] L.Lista,[28] Z.A.Liu,[7] W.Lohmann,[46] E.Longo,[38] Y.S.Lu,[7] K.Lübelsmeyer,[1] C.Luci,[38] D.Luckey,[14] L.Luminari,[38] W.Lustermann,[47] W.G.Ma,[21] L.Malgeri,[20] A.Malinin,[27] C.Maña,[24] D.Mangeol,[30] J.Mans,[36] J.P.Martin,[23] F.Marzano,[38] K.Mazumdar,[10] R.R.McNeil,[6] S.Mele,[18,28] L.Merola,[28] M.Meschini,[17] W.J.Metzger,[30] A.Mihul,[12] H.Milcent,[18] G.Mirabelli,[38] J.Mnich,[1] G.B.Mohanty,[10] G.S.Muanza,[23] A.J.M.Muijs,[2] B.Musicar,[40] M.Musy,[38] S.Nagy,[16] M.Napolitano,[28] F.Nessi-Tedaldi,[47] H.Newman,[31] T.Niessen,[1] A.Nisati,[38] H.Nowak,[46] R.Ofierzynski,[47] G.Organtini,[38] C.Palomares,[18] D.Pandoulas,[1] P.Paolucci,[28] R.Paramatti,[38] G.Passaleva,[17] S.Patricelli,[28] T.Paul,[11] M.Pauluzzi,[32] C.Paus,[14] F.Pauss,[47] M.Pedace,[38] S.Pensotti,[26] D.Perret-Gallix,[4] B.Petersen,[30] D.Piccolo,[28] F.Pierella,[9] P.A.Piroué,[36] E.Pistolesi,[26] V.Plyaskin,[27] M.Pohl,[20] V.Pojidaev,[17] H.Postema,[14] J.Pothier,[18] D.O.Prokofiev,[44] D.Prokofiev,[33] J.Quartieri,[39] G.Rahal-Callot,[47] M.A.Rahaman,[10] P.Raics,[16] N.Raja,[10] R.Ramelli,[47] P.G.Rancoita,[26] R.Ranieri,[17] A.Raspereza,[46] P.Razis,[29] D.Ren,[47] M.Rescigno,[38] S.Reucroft,[11] S.Riemann,[46] K.Riles,[3] B.P.Roe,[3] L.Romero,[24] A.Rosca,[8] S.Rosier-Lees,[4] S.Roth,[1] C.Rosenbleck,[1] B.Roux,[30] J.A.Rubio,[18] G.Ruggiero,[17] H.Rykaczewski,[47] A.Sakharov,[47] S.Saremi,[6] S.Sarkar,[38] J.Salicio,[18] E.Sanchez,[24] M.P.Sanders,[30] C.Schäfer,[18] V.Schegelsky,[33] S.Schmidt-Kaerst,[1] D.Schmitz,[1] H.Schopper,[48] D.J.Schotanus,[30] G.Schwering,[1] C.Sciacca,[28] L.Servoli,[32] S.Shevchenko,[31] N.Shivarov,[41] V.Shoutko,[27,14] E.Shumilov,[27] A.Shvorob,[31] T.Siedenburg,[1] D.Son,[42] P.Spillantini,[17] M.Steuer,[14] D.P.Stickland,[36] B.Stoyanov,[41] A.Straessner,[18] K.Sudhakar,[10] G.Sultanov,[41] L.Z.Sun,[21] S.Sushkov,[8] H.Suter,[47] J.D.Swain,[11] Z.Szillasi,[25,¶] X.W.Tang,[7] P.Tarjan,[16] L.Tauscher,[5] L.Taylor,[11] B.Tellili,[23] D.Teyssier,[23] C.Timmermans,[30] Samuel C.C.Ting,[14] S.M.Ting,[14] S.C.Tonwar,[10,18] J.Tóth,[13] C.Tully,[36] K.L.Tung,[7] Y.Uchida,[14] J.Ulbricht,[47] E.Valente,[38] R.T.Van de Walle,[30] V.Veszpremi,[25] G.Vesztergombi,[13] I.Vetlitsky,[27] D.Vicinanza,[39] G.Viertel,[47] S.Villa,[37] M.Vivargent,[4] S.Vlachos,[5] I.Vodopianov,[33] H.Vogel,[34] H.Vogt,[46] I.Vorobiev,[3427] A.A.Vorobyov,[33] M.Wadhwa,[5] W.Wallraff,[1] M.Wang,[14] X.L.Wang,[21] Z.M.Wang,[21] M.Weber,[1] P.Wienemann,[1] H.Wilkens,[30] S.X.Wu,[14] S.Wynhoff,[36] L.Xia,[31] Z.Z.Xu,[21] J.Yamamoto,[3] B.Z.Yang,[21] C.G.Yang,[7] H.J.Yang,[3] M.Yang,[7] S.C.Yeh,[50] An.Zalite,[33] Yu.Zalite,[33] Z.P.Zhang,[21] J.Zhao,[21] G.Y.Zhu,[7] R.Y.Zhu,[31] H.L.Zhuang,[7] A.Zichichi,[9,18,19] G.Zilizi,[25,¶] B.Zimmermann,[47] M.Zöller.[1]

1 I. Physikalisches Institut, RWTH, D-52056 Aachen, FRG[§]
III. Physikalisches Institut, RWTH, D-52056 Aachen, FRG[§]
2 National Institute for High Energy Physics, NIKHEF, and University of Amsterdam, NL-1009 DB Amsterdam, The Netherlands
3 University of Michigan, Ann Arbor, MI 48109, USA
4 Laboratoire d'Annecy-le-Vieux de Physique des Particules, LAPP,IN2P3-CNRS, BP 110, F-74941 Annecy-le-Vieux CEDEX, France
5 Institute of Physics, University of Basel, CH-4056 Basel, Switzerland
6 Louisiana State University, Baton Rouge, LA 70803, USA
7 Institute of High Energy Physics, IHEP, 100039 Beijing, China[△]
8 Humboldt University, D-10099 Berlin, FRG[§]
9 University of Bologna and INFN-Sezione di Bologna, I-40126 Bologna, Italy
10 Tata Institute of Fundamental Research, Mumbai (Bombay) 400 005, India
11 Northeastern University, Boston, MA 02115, USA
12 Institute of Atomic Physics and University of Bucharest, R-76900 Bucharest, Romania
13 Central Research Institute for Physics of the Hungarian Academy of Sciences, H-1525 Budapest 114, Hungary[‡]
14 Massachusetts Institute of Technology, Cambridge, MA 02139, USA
15 Panjab University, Chandigarh 160 014, India.
16 KLTE-ATOMKI, H-4010 Debrecen, Hungary[¶]
17 INFN Sezione di Firenze and University of Florence, I-50125 Florence, Italy
18 European Laboratory for Particle Physics, CERN, CH-1211 Geneva 23, Switzerland
19 World Laboratory, FBLJA Project, CH-1211 Geneva 23, Switzerland
20 University of Geneva, CH-1211 Geneva 4, Switzerland
21 Chinese University of Science and Technology, USTC, Hefei, Anhui 230 029, China[△]
22 University of Lausanne, CH-1015 Lausanne, Switzerland
23 Institut de Physique Nucléaire de Lyon, IN2P3-CNRS,Université Claude Bernard, F-69622 Villeurbanne, France
24 Centro de Investigaciones Energéticas, Medioambientales y Tecnologícas, CIEMAT, E-28040 Madrid, Spain[♭]
25 Florida Institute of Technology, Melbourne, FL 32901, USA
26 INFN-Sezione di Milano, I-20133 Milan, Italy
27 Institute of Theoretical and Experimental Physics, ITEP, Moscow, Russia
28 INFN-Sezione di Napoli and University of Naples, I-80125 Naples, Italy
29 Department of Physics, University of Cyprus, Nicosia, Cyprus
30 University of Nijmegen and NIKHEF, NL-6525 ED Nijmegen, The Netherlands
31 California Institute of Technology, Pasadena, CA 91125, USA
32 INFN-Sezione di Perugia and Università Degli Studi di Perugia, I-06100 Perugia, Italy
33 Nuclear Physics Institute, St. Petersburg, Russia
34 Carnegie Mellon University, Pittsburgh, PA 15213, USA
35 INFN-Sezione di Napoli and University of Potenza, I-85100 Potenza, Italy
36 Princeton University, Princeton, NJ 08544, USA
37 University of Californa, Riverside, CA 92521, USA
38 INFN-Sezione di Roma and University of Rome, "La Sapienza", I-00185 Rome, Italy
39 University and INFN, Salerno, I-84100 Salerno, Italy
40 University of California, San Diego, CA 92093, USA
41 Bulgarian Academy of Sciences, Central Lab. of Mechatronics and Instrumentation, BU-1113 Sofia, Bulgaria
42 The Center for High Energy Physics, Kyungpook National University, 702-701 Taegu, Republic of Korea
43 Utrecht University and NIKHEF, NL-3584 CB Utrecht, The Netherlands
44 Purdue University, West Lafayette, IN 47907, USA
45 Paul Scherrer Institut, PSI, CH-5232 Villigen, Switzerland
46 DESY, D-15738 Zeuthen, FRG
47 Eidgenössische Technische Hochschule, ETH Zürich, CH-8093 Zürich, Switzerland
48 University of Hamburg, D-22761 Hamburg, FRG
49 National Central University, Chung-Li, Taiwan, China
50 Department of Physics, National Tsing Hua University, Taiwan, China
§ Supported by the German Bundesministerium für Bildung, Wissenschaft, Forschung und Technologie
‡ Supported by the Hungarian OTKA fund under contract numbers T019181, F023259 and T024011.
¶ Also supported by the Hungarian OTKA fund under contract number T026178.
♭ Supported also by the Comisión Interministerial de Ciencia y Tecnología.
♯ Also supported by CONICET and Universidad Nacional de La Plata, CC 67, 1900 La Plata, Argentina.
△ Supported by the National Natural Science Foundation of China.

$\sqrt{s}$ (GeV)	202.8	203.8	205.1	206.3	206.6	208.0	208.6
Luminosity (pb^{-1})	2.7	7.6	68.1	66.9	63.7	8.2	0.1

Table 1: The average centre-of-mass energies and the corresponding integrated luminosities of the data samples collected in the year 2000.

	Mass hypothesis					
$200 \leq \sqrt{s} \leq 209$ GeV	$m_{\mathrm{H}} = 110$ GeV			$m_{\mathrm{H}} = 115$ GeV		
Selection	N_D	N_B	N_S	N_D	N_B	N_S
$\mathrm{Hq\bar{q}}$	49	51.5	11.7	12	9.4	1.8
$\mathrm{H}\nu\bar{\nu}$	13	10.7	3.3	5	3.3	0.66
$\mathrm{He^+e^-}$	0	0.66	0.58	0	0.38	0.14
$\mathrm{H}\mu^+\mu^-$	0	0.38	0.45	0	0.26	0.11
$\mathrm{H}\tau^+\tau^-$	0	0.53	0.19	1	0.14	0.03
$\tau^+\tau^-\mathrm{q\bar{q}}$	3	2.3	0.51	0	0.84	0.15
Total	65	66.1	16.7	18	14.3	2.9

Table 2: The number of observed candidates (N_D), expected background (N_B) and expected signal (N_S) events for the data collected in the year 2000, after a cut on the final discriminant corresponding to a signal-to-background ratio greater than 0.05. This cut is used to calculate the confidence levels.

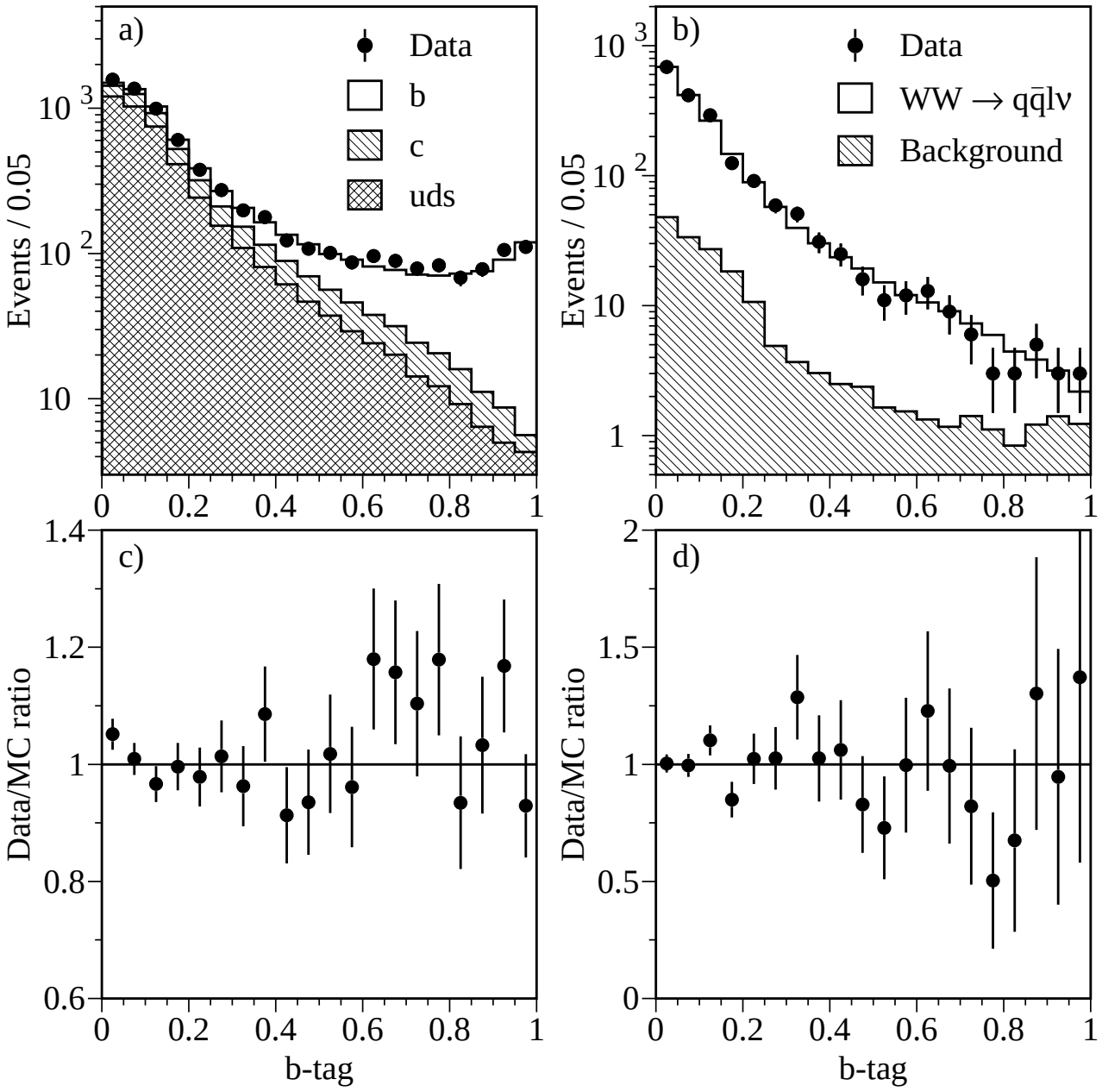

Figure 1: Distribution of the b-tag variable for jets in a sample of a) $e^+e^- \to q\bar{q}(\gamma)$ and b) $W^+W^- \to q\bar{q}\ell\bar{\nu}$ events selected from the high-energy data collected in the year 2000. The data are compared to the simulation of Standard Model processes. The bin-by-bin ratio of the data to the simulated events is displayed in c) and d).

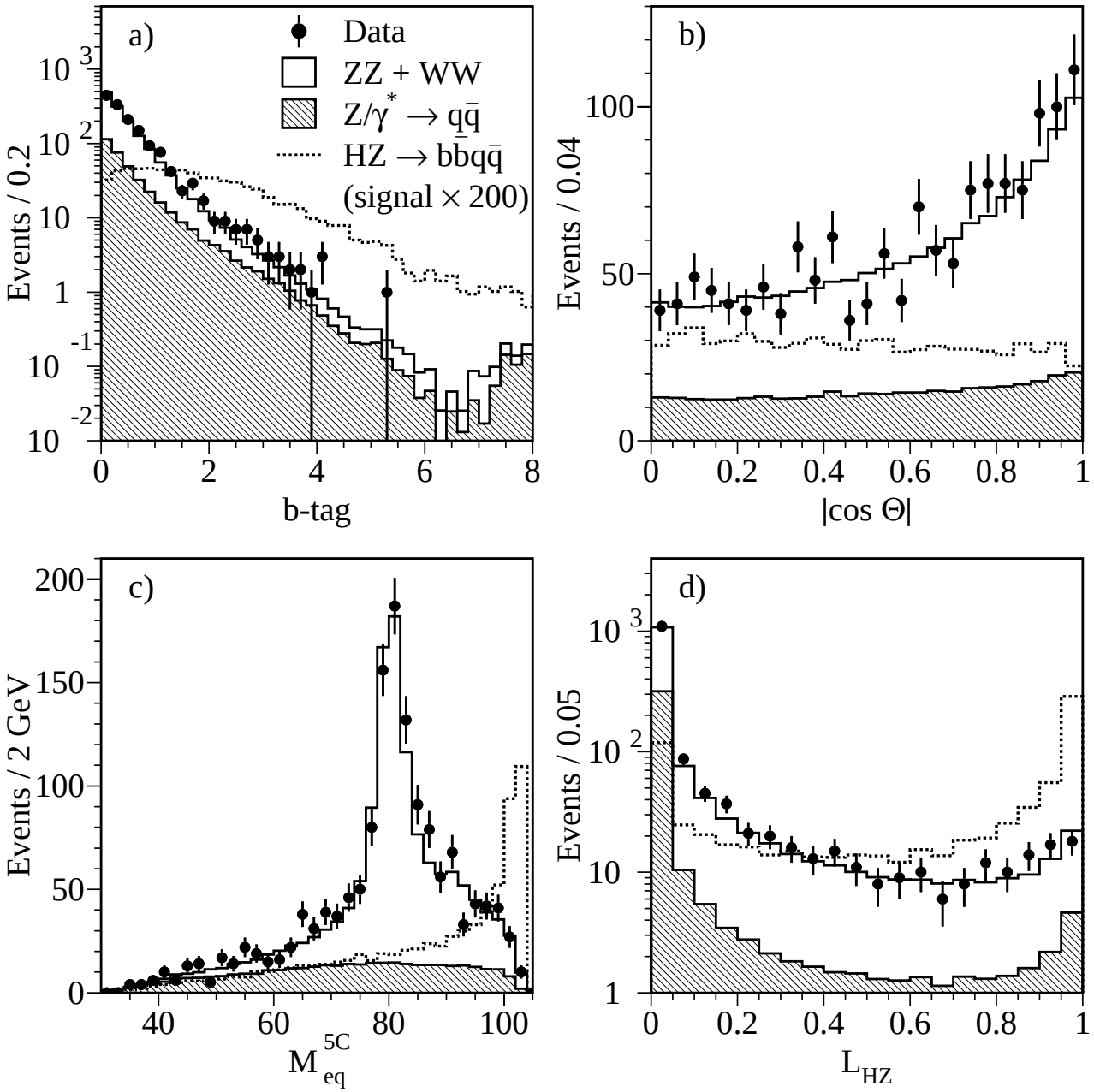

Figure 2: Distribution of a) the b-tag, b) the cosine of the boson production angle, c) the mass from the 5C equal-mass fit and d) the likelihood for the events selected in the Hq$\bar{\text{q}}$ search channel. The points correspond to the data collected at $\sqrt{s} > 206$ GeV. The open and hatched histograms are the expected backgrounds from Standard Model processes. The dashed line is the distribution expected for a 115 GeV Higgs signal, multiplied by a factor of 200.

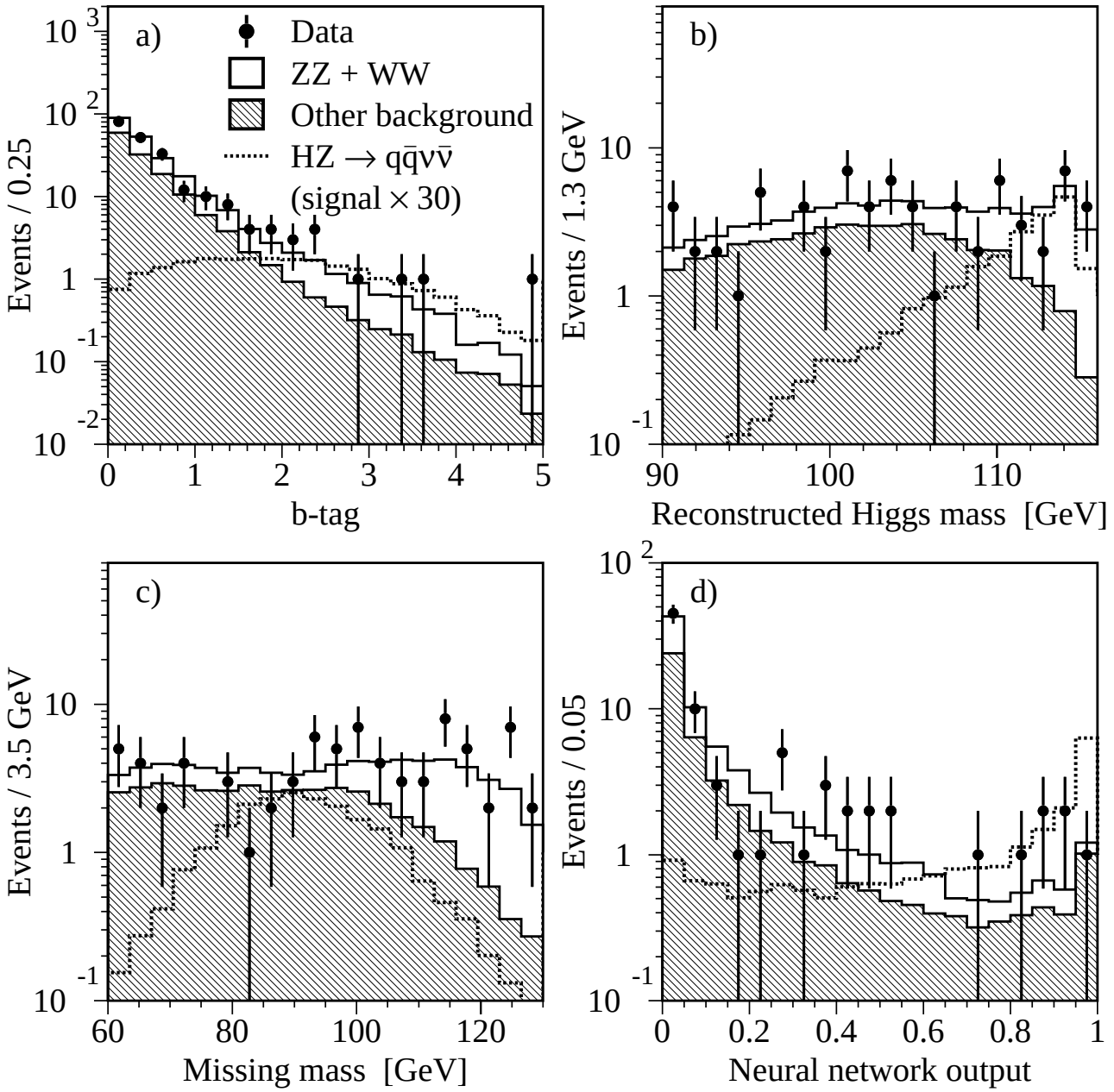

Figure 3: Distribution of a) the b-tag, b) the reconstructed Higgs mass, c) the missing mass and d) the neural network output, for the events selected in the H$\nu\bar{\nu}$ search channel. The points represent the data collected at $\sqrt{s} > 206$ GeV. The open and hatched histograms are the expected backgrounds. The dashed line is the expected Higgs signal with $m_{\mathrm{H}} = 115$ GeV, multiplied by a factor of 30.

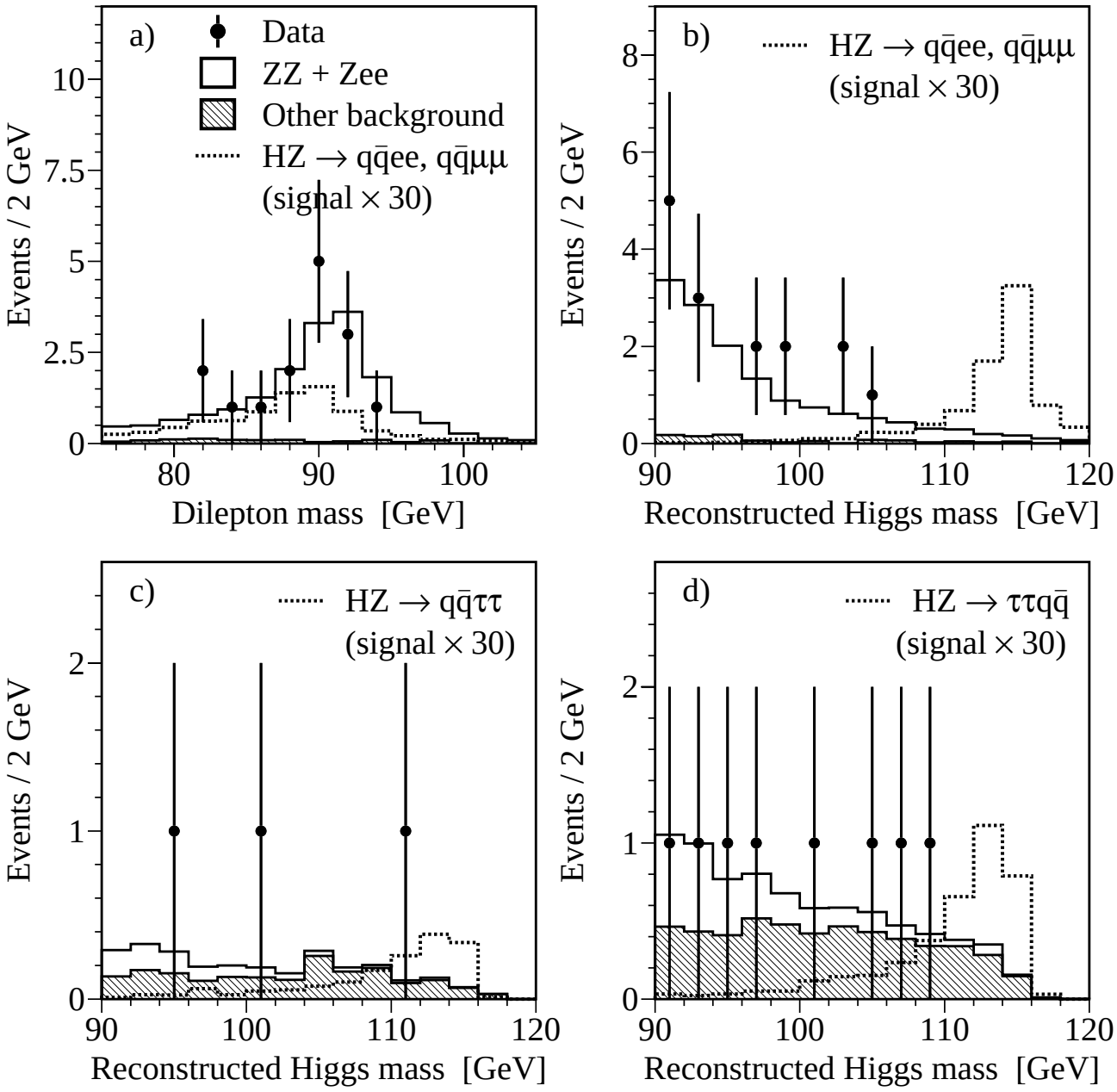

Figure 4: Distributions of a) the dilepton mass and the reconstructed Higgs mass in the b) He^+e^- and $H\mu^+\mu^-$, c) $H\tau^+\tau^-$ and d) $\tau^+\tau^-q\bar{q}$ channels. The points are the data and the open and hatched histograms the expected backgrounds. The dashed line is the expected Higgs signal with $m_H = 115$ GeV, multiplied by a factor of 30, in each channel.

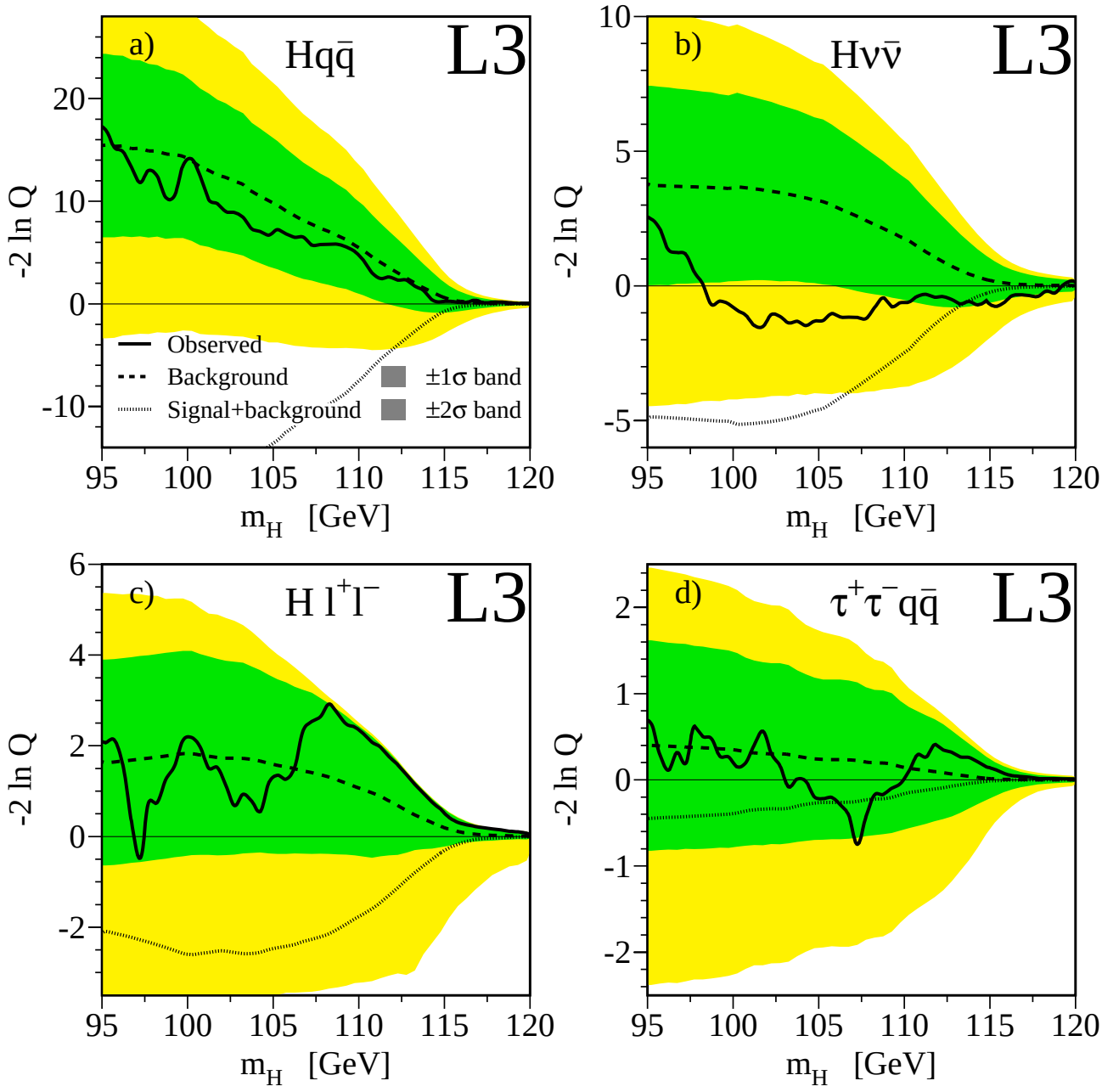

Figure 5: The log-likelihood ratio, $-2\ln Q$, as a function of the Higgs mass hypothesis, m_{H}, for the search channels a) $\mathrm{Hq\bar{q}}$, b) $\mathrm{H}\nu\bar{\nu}$, c) $\mathrm{H}\ell^+\ell^-$ and d) $\tau^+\tau^-\mathrm{q\bar{q}}$. The solid line shows the observed $-2\ln Q$. The dashed line shows the expected median value of $-2\ln Q$ for the "background-only" hypothesis. The dark and light shaded bands show the 68% and 95% probability intervals centred on the background expected median value. The dotted line is the median expected value for the "signal+background" hypothesis.

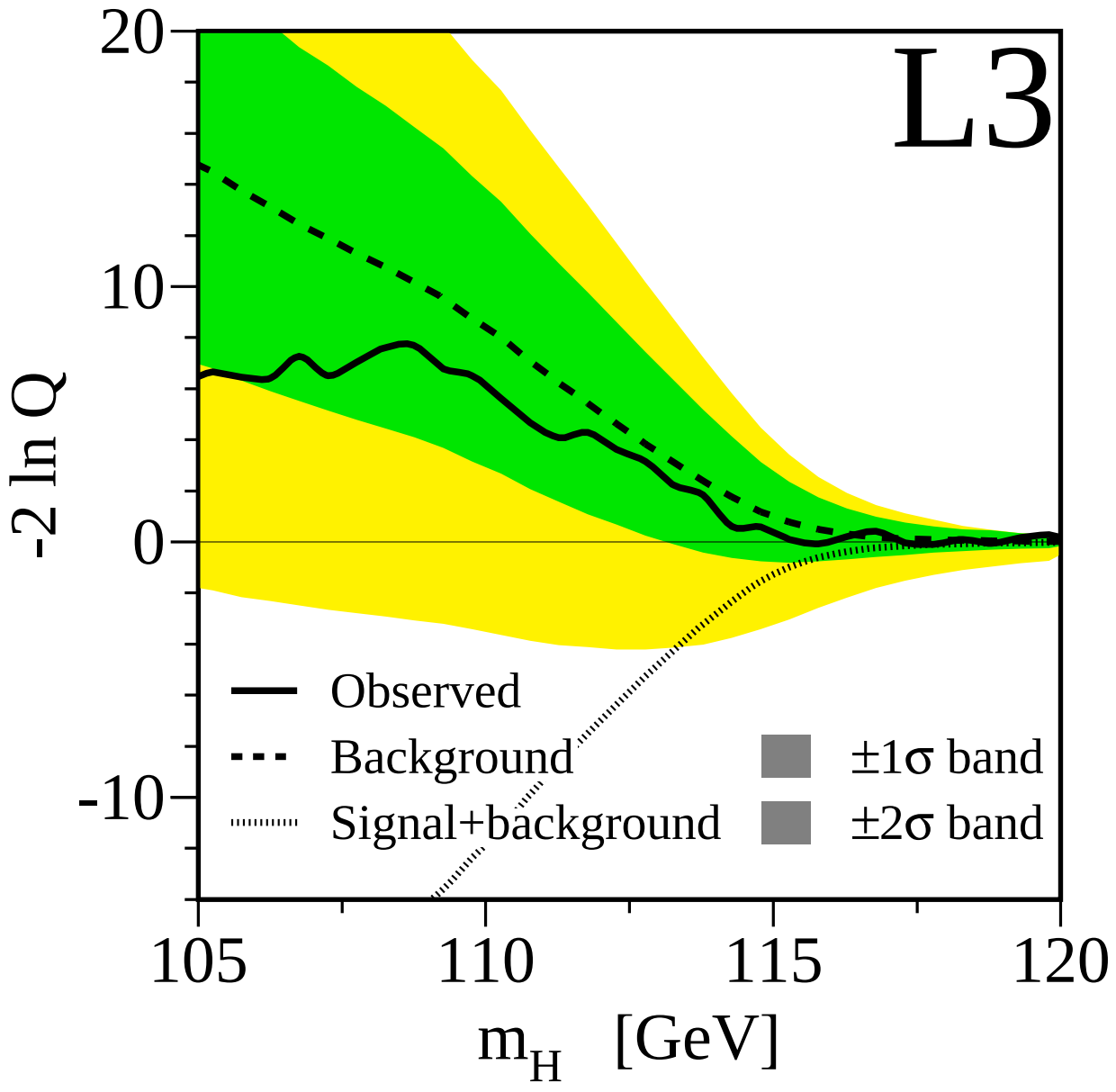

Figure 6: The log-likelihood ratio, $-2\ln Q$, as a function of the Higgs mass hypothesis, m_{H}, for all the search channels combined. The solid line shows the observed $-2\ln Q$. The dashed line shows the expected median value of $-2\ln Q$ for the "background-only" hypothesis. The dark and light shaded bands show the 68% and 95% probability intervals centred on the background expected median value. The dotted line is the median expected value for the "signal+background" hypothesis.

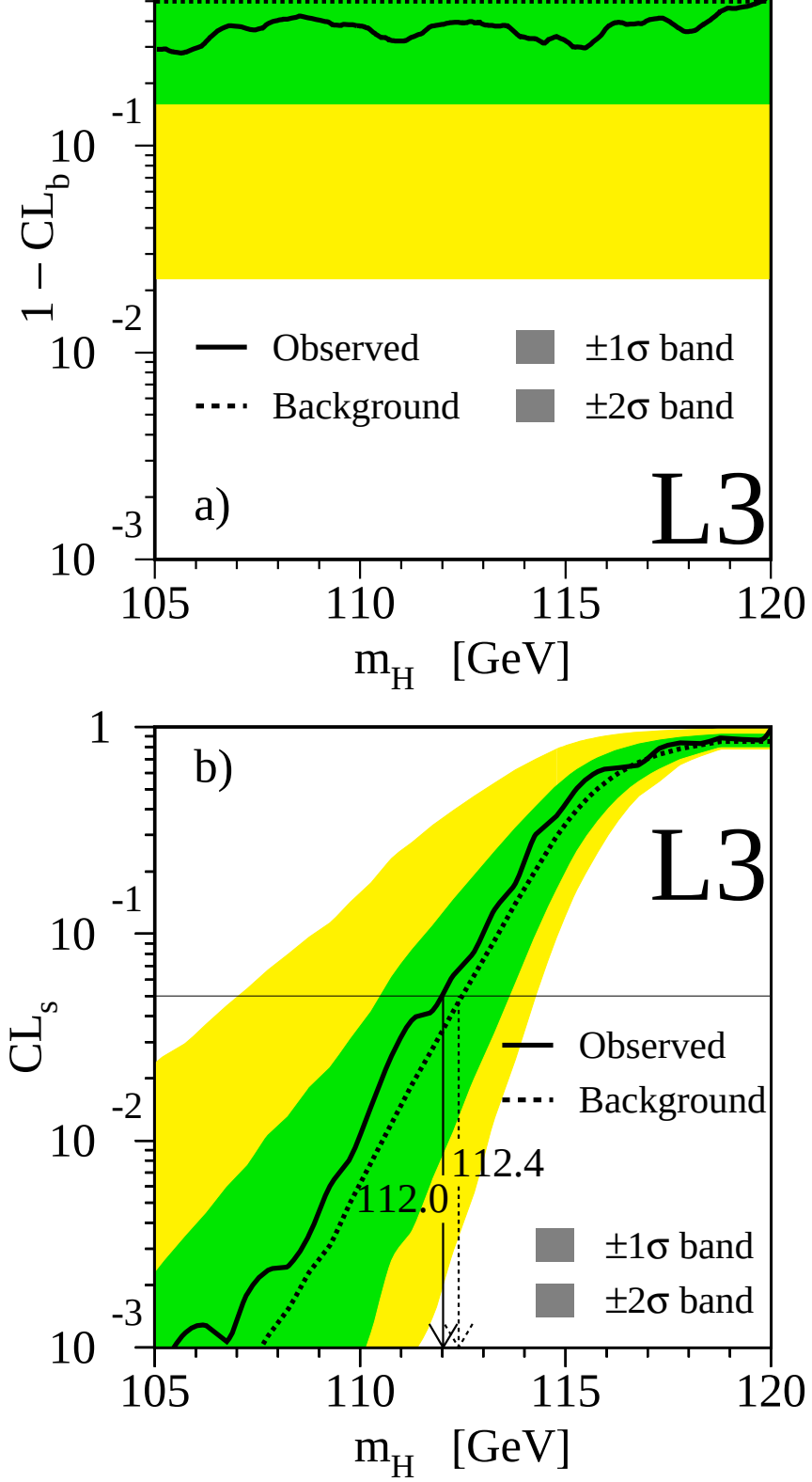

Figure 7: a) The background confidence level $1 - \mathrm{CL}_b$ and b) the signal confidence level, CL_s, as a function of the Higgs mass hypothesis, m_{H}, for all the search channels combined. The data collected at $189 \leq \sqrt{s} \leq 202$ GeV [5, 6] are also included in the combination. The solid line shows the observed value. The dashed line shows the median expected value in a large number of simulated "background-only" experiments. The dark and light shaded bands show the expected 68% and 95% probability intervals centred on the background expected median value. The observed lower limit on the Higgs mass is set at 112.0 GeV, with an expected median value of 112.4 GeV, at the 95% confidence level.